OBSERVATIONS OF THE THERMAL STRUCTURE AND DYNAMICS OF THE MARTIAN ATMOSPHERE.

B. J. Conrath[1], J. C. Pearl[2], M. D. Smith[2], D. Banfield[3], and P. R. Christensen[4], [1]Cornell University, 11805 Haven Hill Dr., Smithsburg, MD 21783, e-mail: barney@chryse.gsfc.nasa.gov, [2]NASA/GSFC, Greenbelt, MD 20771, [3]Cornell University, Space Sciences Building, Ithaca, NY 14853, [4]Geology Dept., Arizona Sate University, Tempe, AZ 85287.

Introduction: Information on the thermal structure of the Martian atmosphere has been obtained using several different techniques, including in situ sounding from decent probes, radio occultations and infrared thermal emission measurements from orbiters, and earth based full-disk microwave measurements. Knowledge of the 3-dimensional atmospheric temperature field and its temporal variation provides an important observational approach to the study of the dynamics of the atmosphere. Comparison of the observed thermal structure with results from a Mars General Circulation Model (MGCM) can be used to refine the model and provide greater insight into the physical processes controlling the dynamics of the atmosphere. Direct assimilation of the temperature observations into an MGCM can also be used to address similar goals. In addition, relatively simple diagnostic models can be applied to the data to directly obtain information on winds and other meteorological properties of the atmosphere.

In this overview, we concentrate primarily on the structure retrieved from thermal emission measurements. This approach has been used extensively to obtain temperature profiles from terrestrial meteorological satellites and has been applied to the atmospheres of other planets. For Mars, measurements in the 15-μm (667 cm^{-1}) CO_2 absorption band are used. During the 1971 global dust storm and its subsequent dissipation, Mariner 9 IRIS spectra were inverted to obtain temperature profiles [1, 2, 3, 4]. Information on a single, relatively thick atmospheric layer centered near the 0.5 mbar level was obtained with the Viking Infrared Thermal Mapper (IRTM) using a single-channel broadband measurement in the CO_2 band [5, 6, 7]. Recently, the Thermal Emission Spectrometer (TES) has obtained extensive new thermal structure information; these results will be the primary focus of this summary.

The TES instrument consists of a Michelson interferometer, along with solar albedo and broadband thermal channels [8]. The interferometer measures the thermal emission spectrum between 200 and 1600 cm^{-1} with nominal selectable spectral resolutions of 5 and 10 cm^{-1}. The individual pixels of the 2x3 detector array subtend 8.3 mrad. The nadir as well as the forward and aft limbs can be viewed using a pointing mirror. Cold space and an onboard blackbody are used for calibration. During the extended aerobraking and science phasing portions of the MGS mission, slightly more than one half of a Martian seasonal cycle was observed, beginning just after northern hemisphere autumnal equinox, through winter solstice, into northern hemisphere spring (L_s = 184-28, where L_s is the aerocentric longitude of the sun). During this time period, approximately 2.4 million temperature profiles were obtained by inversion of TES spectra [9, 10]. These were primarily from nadir-viewing measurements, with a small number of limb spectra acquired near periapsis. Simultaneous retrievals of the infrared optical depth of suspended atmospheric dust were also obtained in many cases. This set of TES retrievals provides the most extensive spatial and temporal coverage yet obtained during this portion of the seasonal cycle. The coverage is essentially global in nature, but more nearly complete in longitude and local time in the southern hemisphere.

Zonal mean structure, as measured by TES, is presented for both equinoxes and the northern hemisphere winter solstice. The results are used in simple diagnostic models to estimate the baroclinic component of the zonal wind field and to make qualitative inferences concerning the meridional circulation. Temperature variances are used to characterize the distribution of planetary scale wave activity, and an analysis of observable wave modes including thermal tides is summarized. Several regional dust storms were observed during the period covered, including the Noachis Terra event in late November 1997. Correlation of the thermal structure with dust activity is examined.

Seasonal Evolution of Atmospheric Structure: During the time period examined here, the MGS spacecraft was in a highly elliptical orbit with the apoapsis at mid to high northern latitudes. As a result, the projection of an individual detector field of view on the planet varied from less than 10 km near periapsis to several hundred km near apoapsis. Coverage in the northern hemisphere during the periapsis pass was confined to two regions about 12 hours and 180° apart in local time and longitude, while in the southern hemisphere at higher latitudes, coverage in local time and longitude is more nearly complete.

Northern hemisphere autumnal equinox. Temperatures profiles from the period L_s = 190-200 were averaged in 2° latitude bins to produce an estimate of a zonal and temporal mean meridional thermal cross section (Fig. 1). An average of the surface pressures for each bin is shown. The zonal wind field (Fig. 2) is estimated from the temperature field assuming gradient wind balance in the horizontal and hydrostatic balance in the vertical, resulting in the thermal wind relation which gives the vertical derivative of the zonal wind. It is assumed that the wind speed is zero at the planetary surface, and the thermal wind relation is integrated upward from the surface, yielding the baroclinic component of the wind field. Any non-vanishing surface wind or barotropic component

must be added to the winds shown in Fig. 2 to obtain the total wind field.

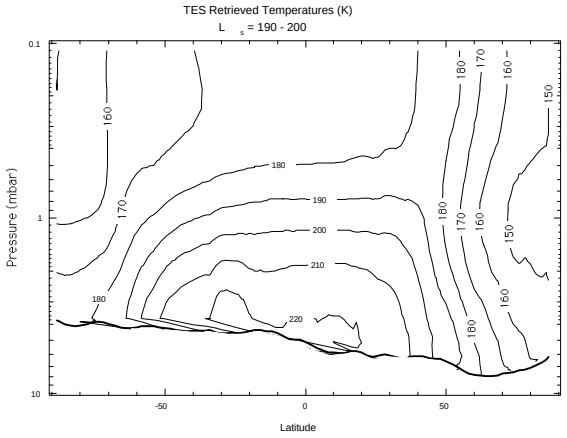

Fig. 1. Zonal mean meridional temperature cross section for near northern hemisphere autumnal equinox.

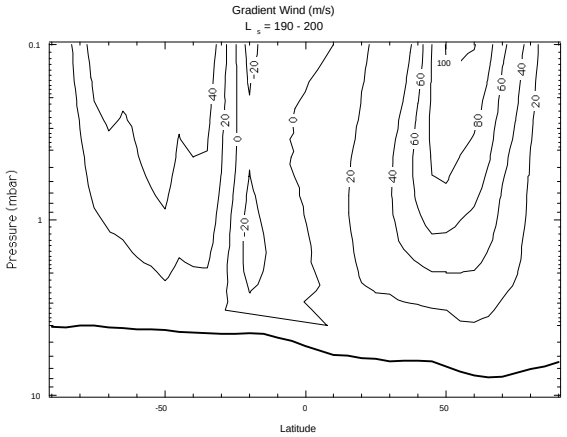

Fig. 2. Gradient thermal wind cross section for near northern hemisphere autumnal equinox.

The temperature and winds for this period show significant hemispheric asymmetry even though it is only a short time after the northern hemisphere autumnal equinox. The latitude temperature gradient poleward of 50 N is associated with the westerly jet, dominating the northern hemisphere flow. In contrast, the southern hemisphere winds are weaker, with westerly winds poleward of about 25 S achieving speeds less than half those of the north. At low southern latitudes, weak easterlies are observed. Examination of Fig. 1 suggests that the mean meridional temperature cannot be in radiative equilibrium, and must be significantly modified by dynamics. Presumably, the temperature maximum at mid-northern latitudes results from adiabatic heating associated with the descending branch of the mean meridional residual (Hadley) circulation, with upward motion near subsolar latitudes. The southern hemisphere meridional circulation appears to be significantly weaker.

Northern hemisphere winter solstice. The mean meridional cross section for L_s = 190-200 is shown in Fig. 3 and the corresponding gradient thermal wind cross section is shown in Fig. 4. Under winter solstice conditions, the westerly jet in the northern hemisphere has intensified and become more confined in latitude, resulting in a strong circum-polar vortex. Near 0.1 mbar (the upper boundary of the region accessible to TES nadir measurements) wind speeds exceeding 100 m s^{-1} are observed. At high northern latitudes, the temperature maximum aloft has become stronger relative to the autumnal equinox conditions; this suggests an intensification of the meridional circulation, resulting in an increase in adiabatic heating.

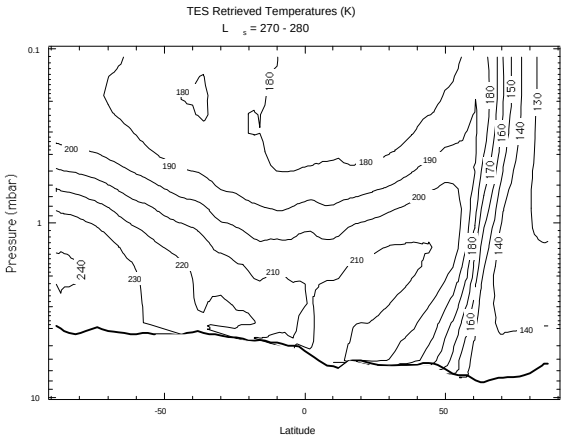

Fig. 3. Zonal mean meridional temperature cross section for near northern hemisphere winter solstice.

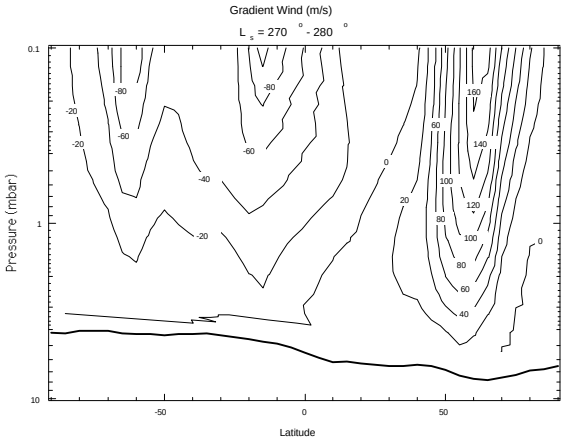

Fig. 4. Gradient thermal wind cross section for northern hemisphere winter solstice.

The adiabatic heating due to the decent of the Hadley cell at high northern latitudes, combined with strong radiative cooling of the north polar atmosphere, maintains the strong latitude temperature gradients observed in the region centered near 60 N. Maximum temperatures in the southern hemisphere occur near the south pole, resulting in generally increasing temperatures from the equator to the pole. Consequently, the winds are predominantly easterly in this hemisphere. Again, the observed meridional temperature structure deviates strongly from radiative equilibrium, and is consistent with a sol-

stitial cross equatorial Hadley circulation extending from high southern latitudes, where strong diurnally integrated solar heating is occurring, to high northern latitudes [11, 12, 13].

The observed structure and wind field appear to be in reasonable qualitative agreement with published model results. For example, Haberle et al. [12] show results for the period L_s = 255-286 that can be compared with the TES data. During the time of the observations, the 9-μm dust optical depths retrieved from the TES data were near 0.2 [14]; if the ratio of visible to 9-μm optical depth is assumed to be 2.5 [15], the appropriate visible optical depth would be about 0.5. The observed thermal structure appears to be essentially bracketed by the model results for optical depths of 0.3 and 1.0, but are somewhat closer to the case for an optical depth of 1.0. The general features of the derived thermal winds agree with model results except for a westerly jet at low levels centered near 30 S that is seen in the model. Since this jet results from the near-angular momentum conserving southward flow of the lower branch of the Hadley circulation [12, 16], it can be regarded as a barotropic component of the flow not accessible to the thermal wind calculation.

Northern spring equinox. The mean meridional thermal structure for L_s = 2-4, just after northern spring equinox, is shown in Fig. 5 with the corresponding gradient thermal winds shown in Fig. 6. As in the case of the autumnal equinox, the winds are predominantly westerly in both hemispheres; however, some asymmetry remains, with stronger winds in the northernhemisphere.

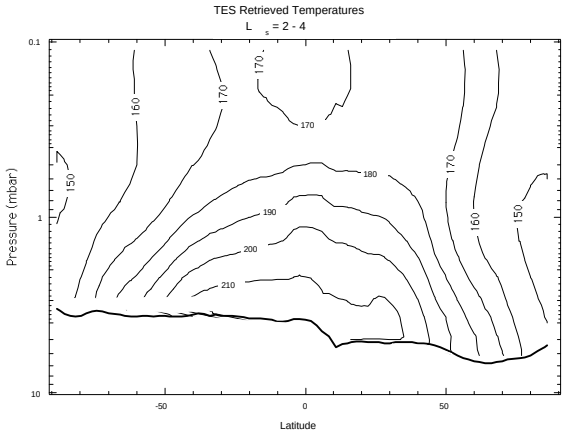

Fig. 5. Zonal mean meridional temperature cross section for northern hemisphere spring equinox.

The model results of Haberle et al. [12] for the period L_s = 0-23 and a visible dust optical depth of 0.3 show general magnitudes of the temperatures and winds comparable to the observations. The model shows considerable symmetry in the region between approximately 40 S and 40 N, but at higher latitudes, temperatures decrease more rapidly toward the pole in the southern hemisphere than in the north. This is in contrast with the observations, which show stronger poleward temperature gradients and higher wind speeds in the north. This difference could be due, at least in part, to the longer time period over which the model results were averaged, extending further into the northern hemisphere spring.

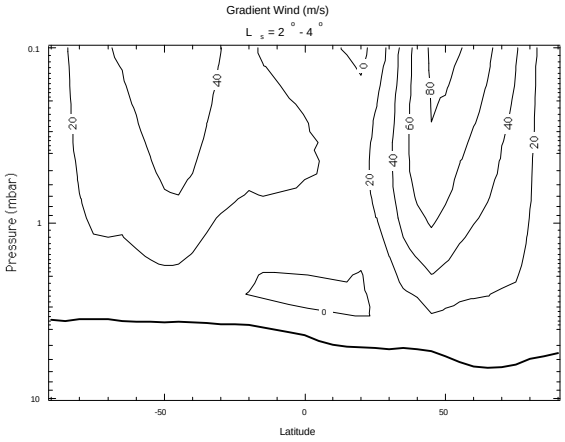

Fig. 6. Gradient thermal wind cross section for northern hemisphere spring equinox.

Dust Storm Behavior: The final period of TES data considered is for L_s = 225-233, corresponding to the time when the Noachis Terra regional dust storm was near its maximum intensity [14]. Although the storm was regional, it had a profound effect on the global thermal structure as can be seen in Fig. 7. A temperature maximum is seen at low levels in the southern hemisphere, centered near 30 S where the atmospheric dust loading is greatest. In the northern hemisphere, a strong temperature maximum is observed near 60 N due to a rapid intensification of the cross-equatorial Hadley circulation and accompanying increased adiabatic heating in the downward branch.

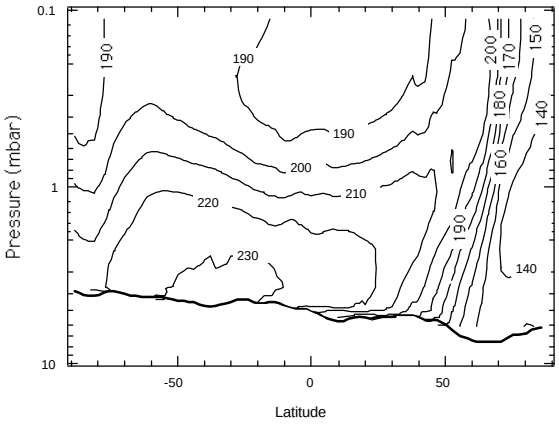

Fig. 7. Zonal mean meridional temperature cross section during the Noachis Terra dust storm.

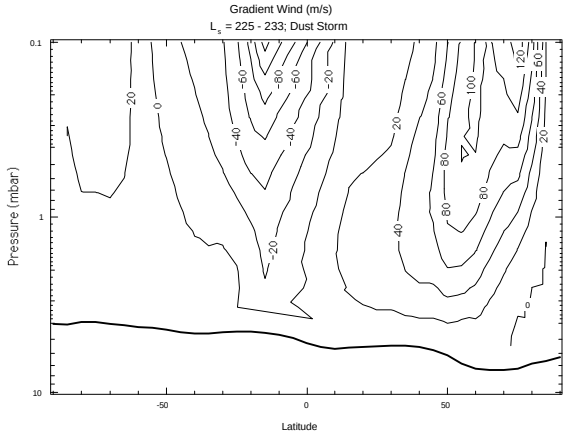

Fig. 8. Gradient thermal wind cross section during the Noachis Terra dust storm.

An intense horizontal temperature gradient lies poleward of the temperature maximum at 60 N. This polar front shows a strong poleward tilt with increasing height, and the core of a strong polar vortex penetrates to 60 N as shown in Fig. 8. A similar rapid enhancement of temperatures at high northern latitudes was observed in the Viking IRTM 15-μm channel data during global dust storm conditions [5, 7]. Several global dust storm numerical simulations have been published [13, 17, 18]. The Noachis storm was regional, never achieving global status, and occurred approximately mid way between equinox and solstice, while the published simulations have been directed primarily at near-global atmospheric dust loading and solstitial seasonal conditions. Nevertheless, the observed thermal structure exhibits behavior qualitatively similar to some of the simulations. The results of Wilson's [13] simulations, for example, show high temperatures aloft poleward of 60 N, along with an intense circumpolar jet at very high latitudes. In the southern hemisphere, the TES temperatures reach a maximum near 60 S and then decrease toward the south pole, rather than the monotonic increase toward the pole displayed by the models. This may be a consequence of the earlier occurrence of the Noachis storm, prior to the establishment of a strong seasonal pole-to-pole meridional circulation.

Waves: Deviations of the thermal structure from the zonal and temporal mean are of major importance in diagnostic studies of atmospheric dynamics. The TES data also yield substantial information on this wave component. Some indication of wave activity and its spatial distribution can be obtained by examining the temperature standard deviations associated with the zonal mean meridional cross sections. As an example, the meridional cross section standard deviation is shown in Fig. 9. The observed pattern for northern winter solstice indicates the presence of wave activity at low and mid latitudes in the southern hemisphere and in a confined latitude range centered near 60 N. In the latter case, the maximum standard deviation occurs just below the 1 mbar level, and the temperatures are highly correlated with the wind field. Examination of this structure indicates that the polar vortex includes planetary scale wave components superposed on the zonal mean jet structure. Weaker wave activity is indicated in the standard deviation cross sections for the equinoxes (not shown).

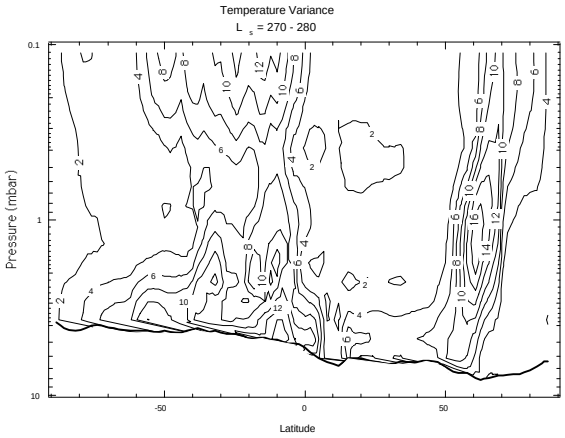

Fig. 9. Standard deviations associated with the zonal mean temperature cross section for the northern winter solstice.

Detailed wave analysis of the thermal structure indicates the presence various planetary scale modes, including diurnal tides in the southern hemisphere where local time coverage is adequate.

Acknowledgments: This work was supported in part by the Mars Global Surveyor Project, the NASA Mars Data Analysis Program, and the JPL Mars Exploration Directorate Science Office.

References: [1] Hanel R. A. et al. (1972) *Icarus, 17*, 423-442. [2] Conrath B. J. (1973) *JGR, 78*, 4267-4278. [3] Conrath B. J. (1975) *Icarus, 24*, 36-46. [4] Conrath B. J. (1981) *Icarus, 48*, 246-255. [5] Martin T. Z. and Kieffer H. H. (1979) *JGR, 84*, 2843-2852. [6] Martin T. Z. (1981) *Icarus, 45*, 427-446. [7] Jakosky B. M. and Martin T. Z. (1987) *Icarus, 72*, 528-534. [8] Christensen P. R. et al. (1992) *JGR, 97*,7719-7734. [9] Christensen P. R. et al. (1998) *Science, 179*, 1692-1698. [10] Conrath B. J. et al. (1999) submitted to *JGR*. [11] Schneider E. K. (1983) *Icarus, 55*, 302-331. [12] Haberle R. M. et al. (1993) *JGR, 98*, 3093-3123. [13] Wilson J. R. (1997) *Geophys. Res. Lett., 24*, 123-126. [14] Smith M. D. et al. (1999) *JGR*, submitted. [15] Martin T. Z. (1986) *Icarus, 66*, 2-21. [16] Wilson J. R. and Hamilton K. (1996) *J. Atmos. Sci., 53*, 1290-1326. [17] Murphy J. R. et al. (1993) *JGR, 98*, 3197-3220. [18] Murphy J. R. et al. (1995) *JGR, 100*, 16357-26376.